COMPONENT PART NOTICE

THIS PAPER IS A COMPONENT PART OF THE FOLLOWING COMPILATION REPORT:

TITLE: Transactions of the Army Conference on Applied Mathematics and Computing (2nd) Held at Washington, DC on 22-25 May 1984.

TO ORDER THE COMPLETE COMPILATION REPORT, USE AD-A154 047.

THE COMPONENT PART IS PROVIDED HERE TO ALLOW USERS ACCESS TO INDIVIDUALLY AUTHORED SECTIONS OF PROCEEDING, ANNALS, SYMPOSIA, ETC. HOWEVER, THE COMPONENT SHOULD BE CONSIDERED WITHIN THE CONTEXT OF THE OVERALL COMPILATION REPORT AND NOT AS A STAND-ALONE TECHNICAL REPORT.

THE FOLLOWING COMPONENT PART NUMBERS COMPRISE THE COMPILATION REPORT:

AD#: P004 902 thru P004 958 AD#:

AD#: AD#:

AD#: AD#:

Accession For	
NTIS GRA&I	☒
DTIC TAB	☐
Unannounced	☐
Justification	
By	
Distribution/	
Availability Codes	
Dist	Avail and/or Special
A-1	

This document has been approved for public release and sale; its distribution is unlimited.

DTIC FORM 463 MAR 85

OPI: DTIC-TID

13-21

JET-CONTAMINANT INTERACTION IN CONFINED GEOMETRIES

Lang-Mann Chang
U.S. Army Ballistic Research Laboratory
Aberdeen Proving Ground, MD 21005

ABSTRACT. A numerical simulation is presented for investigation of the early phase of the flow interaction between a water jet and a chemical contaminant residing in cavities of a wall and in corners of two perpendicular walls. Such a interaction often occurs in surface decontamination processes. The flow model for this analysis is a two-dimensional, two-fluid flow governed by the unsteady Navier-Stokes equations. The equations were solved via finite difference schemes using the SOLA-VOF code. Computer plots of the flow development are presented. The results show that an inclined jet is more effective than a normal jet for decontaminating these confined geometries. In all flow cases studied, the impact pressure on the impingement wall far exceeds the corresponding steady-state dynamic pressure of the jet.

I. INTRODUCTION. Utilization of liquid jet spray is one of the most practical and most effective means for decontaminating Army vehicles in chemical warefare or for surface cleaning in the industry. The prccedure is to use the force produced by the turning of jet stream at the impingement to displace the contaminant.

For a plane wall decontamination using a water jet spray, Chang [1] has characterized the interaction of the jet with the contaminant. In many areas there exist cavities under a surface or corners formed by two perpendicular walls, as depicted in Fig. 1. The chemical contaminant under consideration may reside in these confined geometries in the form of a drop or a layer of fluid covering the entire bottom surface of the geometries.

The flow interaction involves two fluids, the jet fluid (water) and the contaminant, and there is an interface in between, presenting a complex two-fluid problem. To simplify the analysis, we treated the interaction as a two-dimensional flow. The flow field is governed by the unsteady Navier-Stokes equations which were solved numerically via finite difference schemes using the SOLA-VOF computer code [2].

The emphases of this study are on the early evolution of the contaminant drop and the magnitude of the impact pressure on the bottom surfaces of the confined geometries. Computer plots of the flow process are presented. The effect of the angle of jet incidence on the flow is discussed. The results obtained provide useful data for the design of efficient jet sprays used for chemical decontamination.

II. FLOW MODELS AND GOVERNING EQUATIONS. Figs. 2 and 3 are the models of the pre-impingement configurations corresponding to

the schematics presented in Fig. 1. The shaded areas are the regions initially covered by the contaminant and the rest of the space in the geometries is filled with water. The dimensions of the contaminant drops are 3 mm by 0.6 mm, representing the average size of the drops deployed on vehicles. The dimensions of the cavity, however, are representive. A single water jet with a steady and uniform velocity is directed to impinge on the upper surface of the water at an angle of incidence, θ. Two angles, $\theta=45^{o}$ and $\theta=90^{o}$, have been considered. The jet width D_j is 1.83 mm with which a jet can perform decontamination effectively and efficiently [1]. In Figs. 2 and 3 there is a thin water layer covering the contaminant. This layer may exist practically and was found helpful in reducing the numerical instability problem encountered at the water-contaminant interface. Without the layer the stationary and highly viscous contaminant will be in direct contact with the high-speed jet fluid and, as a consequence, there is a great shear stress at the interface.

Fig. 4 shows the flow region and its necessary boundary conditions for the flow analysis in a cavity. An outflow condition is specified at the upper boundary so that the fluids can flow out the region after the start of the jet flow. The setup for the flow analysis in a corner is essentially the same except that an additional outflow condition is prescribed at the left wall.

The governing equations of the above flow models are the continuity equation

$$\frac{1}{\rho c^2}\frac{\partial p}{\partial t} + \frac{\partial u}{\partial x} + \frac{\partial v}{\partial y} = 0 \tag{1}$$

and the momentum equations

$$\frac{\partial u}{\partial t} + u\frac{\partial u}{\partial x} + v\frac{\partial u}{\partial y} = -\frac{1}{\rho}\frac{\partial p}{\partial x} + \nu\left[\frac{\partial^2 u}{\partial x^2} + \frac{\partial^2 u}{\partial y^2}\right] \tag{2}$$

$$\frac{\partial v}{\partial t} + u\frac{\partial v}{\partial x} + v\frac{\partial v}{\partial y} = -\frac{1}{\rho}\frac{\partial p}{\partial y} + \nu\left[\frac{\partial^2 v}{\partial x^2} + \frac{\partial^2 v}{\partial y^2}\right] \tag{3}$$

where t is time, u and v are the x-component and the y-component of the flow velocity, respectively. The density ρ, the sound speed c, and the kinematic viscosity ν are assumed to be constant. Based on the jet width and the jet velocities used in this study, the Reynolds numbers are between 20 and 2000. Within this range, Eqs. (2) and (3) are felt to be appropriate without considering turbulence effects.

For the tracking of the water-contaminant interface, we define a function F called the fractional volume of fluid function, satisfying the relation

$$\frac{\partial F}{\partial t} + u\frac{\partial F}{\partial x} + v\frac{\partial F}{\partial y} = 0 \qquad (4)$$

The value of F in a computational mesh cell is equal to the fractional volume of the cell occupied by the contaminant. Then the value of F is one in cells full of the contaminant and zero in cells containing only water. Cells with F values between zero and one contain an interface, as illustrated in Fig. 5.

In order to adapt the SOLA-VOF code to the present problem involving two fluid with distinct viscosities, we use the following viscosity relation

$$\nu = \nu_c F + (1-F)\nu_w \qquad (5)$$

where ν is the average kinematic viscosity of the fluid mixture in a cell. ν_c and ν_w are the kinematic viscosities of the contaminant and water, respectively. Since the densities of the two fluids are different, the density of the fluid mixture in a cell is approximated as

$$\rho = \rho_c F + (1-F)\rho_w \qquad (6)$$

where ρ_c and ρ_w are the densities of the contaminant and water, respectively.

III. COMPUTATIONAL RESULTS. The jet velocities V_j chosen for computations are 5 and 10 m/s (producing steady-state dynamic pressures of 12.4 kPa and 55 kPa, respectively) which are practical for chemical decontamination. The viscosity of the contaminant under consideration is $\nu_c = 10\,\nu_w$ and the density is $\rho_c = 1.07\,\rho_w$.

The computational results to be presented are in two parts: flow patterns and the impact pressure on the bottom walls of the confined geometries.

Flow Patterns

Fig. 6 shows the flow generated by a water jet impinging on the upper surface of a cavity filled with water and with a contaminant drop initially located at the right corner, as seen in Fig. 2a. It is noted that the computer plots have been magnified three times in the vertical direction in order to provide a clear flow visualization. The plots in the left and the right columns correspond to the 45°- and 90°-impingement, respectively. The flow direction of the main stream in the

cavity is strongly influenced by the angle of jet incidence. In the 45°-impingement, the main stream moves toward the left wall and then turns and exits the cavity, while in the 90°-impingement the main stream exits the cavity adjacent to the entrance of the jet stream. As a result, the contaminant subjected to the 45°-impingement has experienced a larger displacement along the bottom wall than the contaminant subjected to the 90°-impingement. In addition, there is still a small amount of contaminant stagnating at the right corner at 0.3 ms in the 90° case. It is, therefore, obvious that a jet impinging at 45° has more cleaning power for decontaminating the cavity. Fig. 7, which was obtained by using the technique of embedding marker particles in the region initially covered by the contaminant, shows another view of the evolution of the contaminant drop.

In the case that a contaminant drop is initially located at the left corner of a cavity as depicted in Fig. 2b, Figs. 8 and 9 also indicate that the jet impinging at 45° is more effective for cleaning the cavity. There is an interesting flow phenomenon to be noticed in the 45° case. The upward flow velocity near the left wall is greater than the velocity slightly far away the wall. It is attributed to the flow impingement on that wall.

Fig. 10 shows the results corresponding to Fig. 2c in which an impingement takes place in the central part of the cavity. In the 90°-impingement, the main water stream induced by the jet flow does not reach the end walls. Therefore, there is little movement in the contaminant along the right end wall.

Fig. 11 displays the flow development corresponding to the configuration in Fig. 2d in which the cavity is full of contaminant with a thin water layer on the top. At times up to 0.27 ms, the flow patterns for the two angles of jet incidence are similar. However, in the 90° case the movement of the contaminant along the right end wall slows down as time progresses due to a faster development of viscous layer along the wall.

Next, we examine the results for the other kind of confined geometry investigated: the corners shown in Fig. 3. Figs. 12 and 13 present the flow patterns developed from Fig. 3a and Fig. 3b, respectively. The main stream is moving freely to the left because the left end is open to the flow. Though the flow patterns for the two angles of jet incidence are similar in general, the 45° jet exhibits slightly better performance since it cleans up the contaminant in the right corner faster.

Pressure Distribution on the Bottom Wall

The impact pressure on the bottom surfaces of the subject confined geometries is another important datum to be determined. In some critial areas of a vehicle, such as optical windows, the pressure applied without causing damage is limited to a certain level. Figs. 14 through 17 present the resulting ratios of the instantaneous impact pressure to the corresponding steady-state

dynamic pressure which is $1/2(\rho_w V_j^2)$ for various flow configurations. Fig. 14 is the result for the configuration in Fig. 2a, showing that the pressure ratio can reach 13. In the configuration in Fig. 2d, the pressure ratio shown in Fig. 15 is even higher, approximately 19. In the corner flows shown in Figs. 3a and 3b, the corresponding pressure ratios displayed in Figs. 16 and 17, respectively, are relatively lower. It is a result of the change of boundary condition from a noflow to an outflow condition. We also notice that the 45°-impingement produces a slightly higher impact pressure in Figs. 14 and 15 than the 90°-impingement does.

IV. CONCLUSIONS. Computer plots have been generated to show the detailed flow development in the early phase of the jet-contaminant interactions in cavities and corners. Based on the flow patterns, a jet impinging at an appropriate inclined angle, say 45°, is more effective than a normal jet for decontaminating such confined geometries. The instantaneous pressure rise on the bottom surfaces of the confined geometries can far exceed the corresponding steady-state dynamic pressure of the jet. In general, the pressure rise is higher in cavities than in corners.

REFERENCES

1. L. Chang,"Characterization of Jet-Contaminant Interaction Flow in Chemical Decontamination," U.S. Army Ballistic Research Laboratory Technical Report (in press).

2. B. Nicholas, C. Hurt, and R. Hotchkiss,"SOLA-VOF: A Solution Algorithm for Transient Fluid Flow with Multiple Free Boundaries," Los Alamos Scientific Laboratory Report No. LA-8355, 1980.

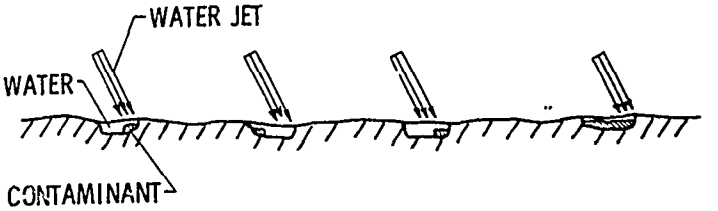

Contaminant in Cavities

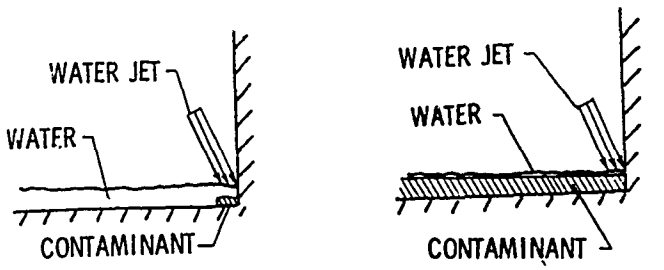

Contaminant in Corners

Fig. 1 Contaminant in Confined Geometries

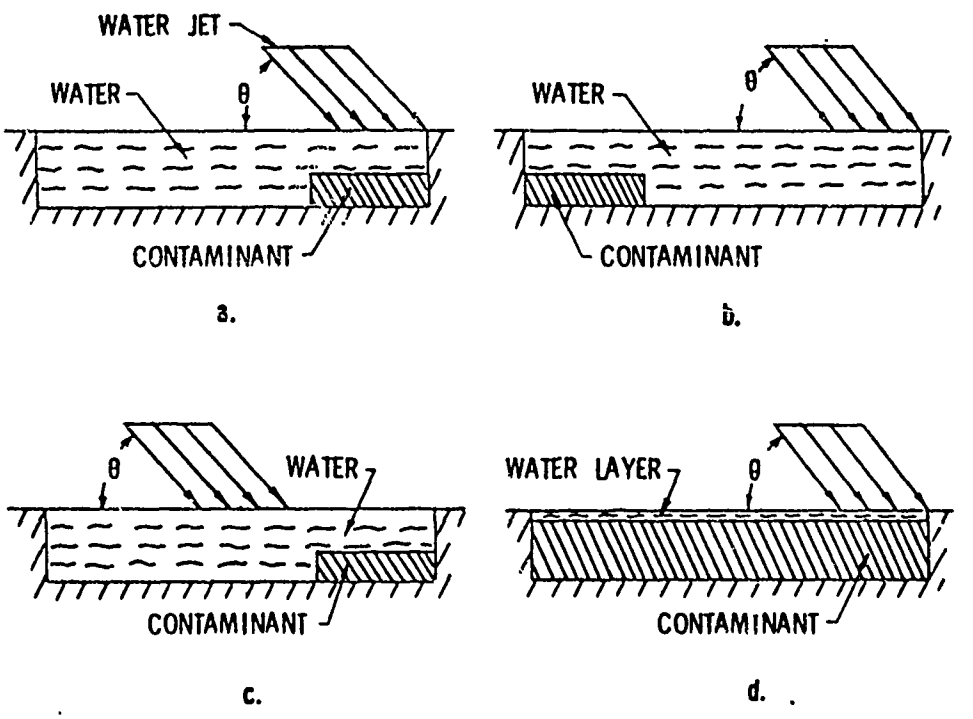

Fig. 2 Pre-impingement Flow Configurations in Cavities

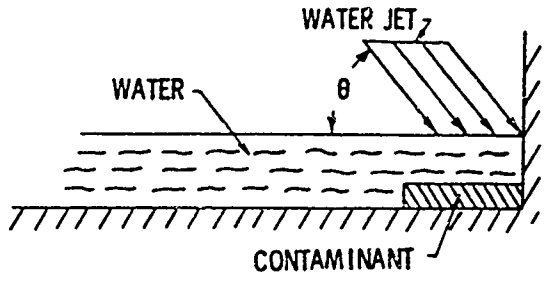

a.

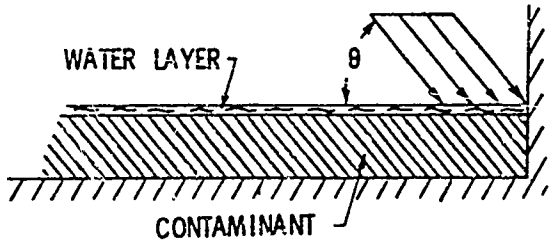

b.

Fig. 3 Pre-impingement Flow Configurations in Corners

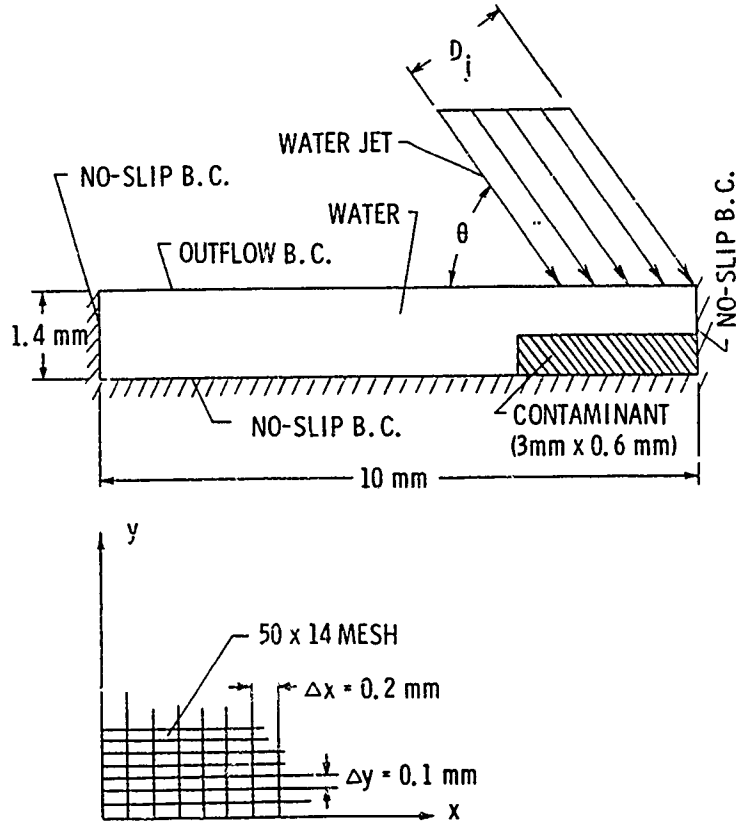

Fig. 4 Flow Region and Boundary Conditions for a Cavity

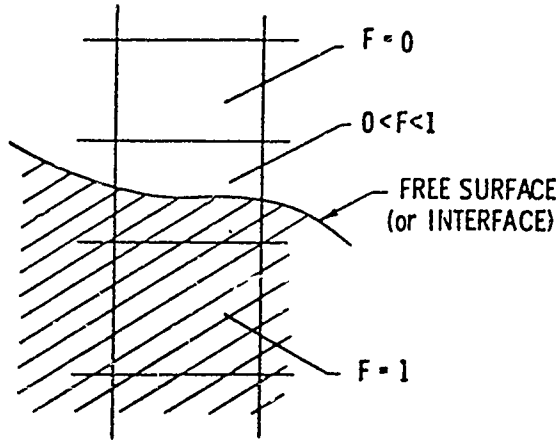

Fig. 5 Free Surface (or Interface) Across a Mesh Cell

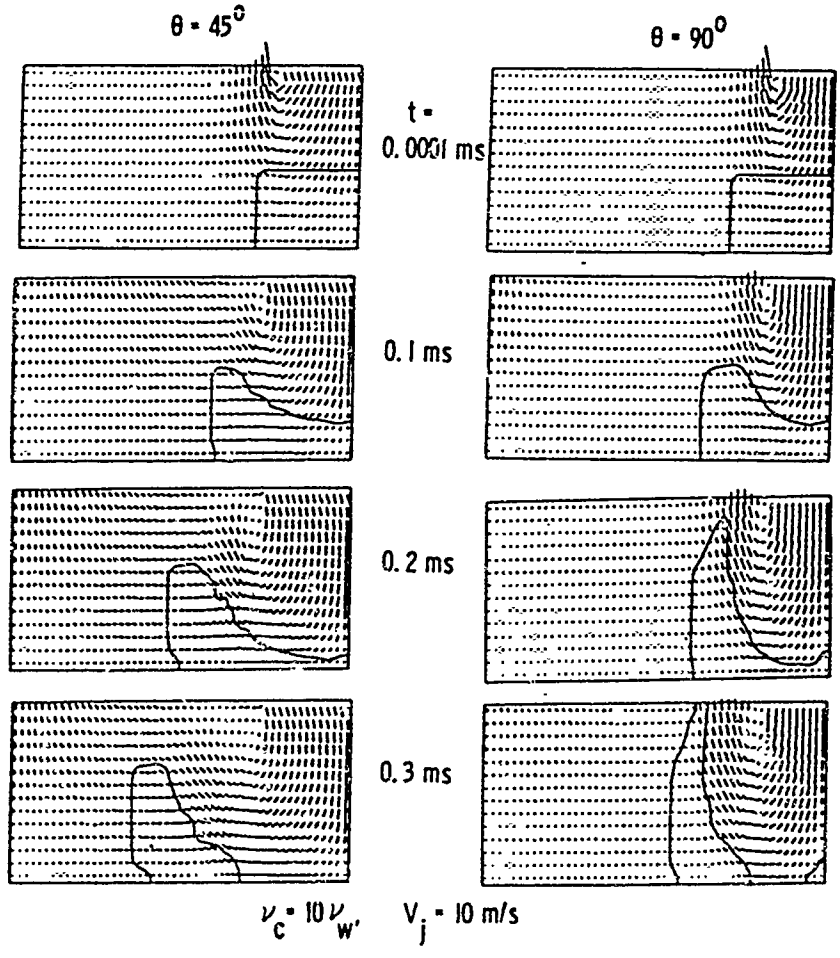

Fig. 6 Flow Development (corresponding to Fig. 2a)

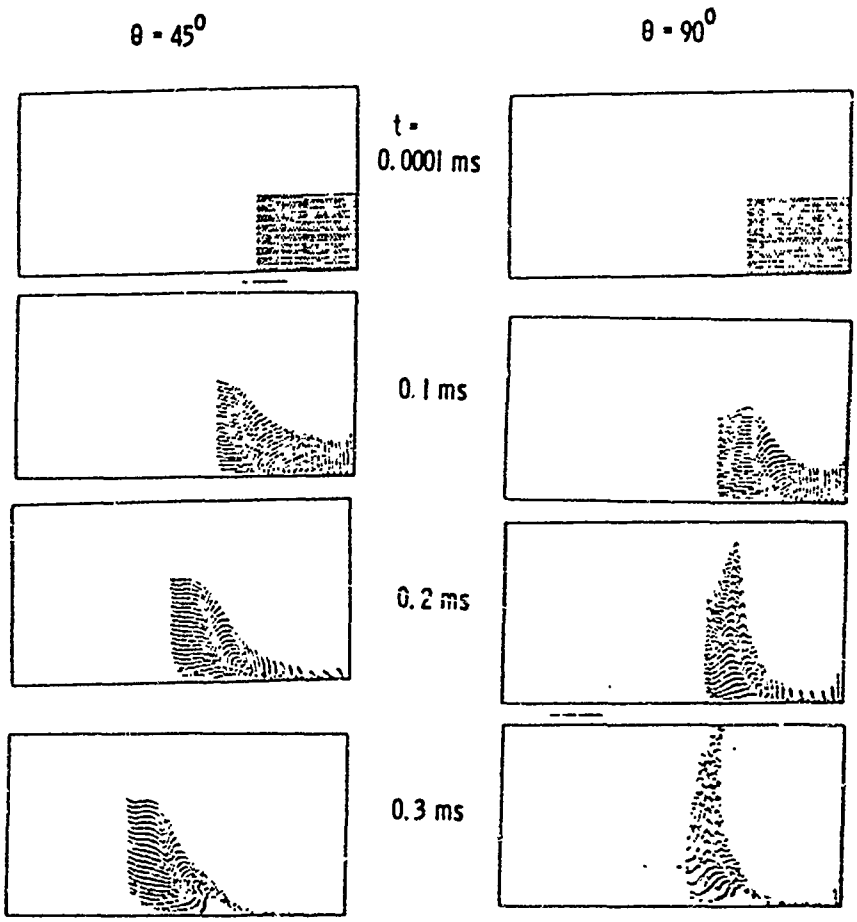

Fig. 7 Evolution of Drops (corresponding to Fig. 6)

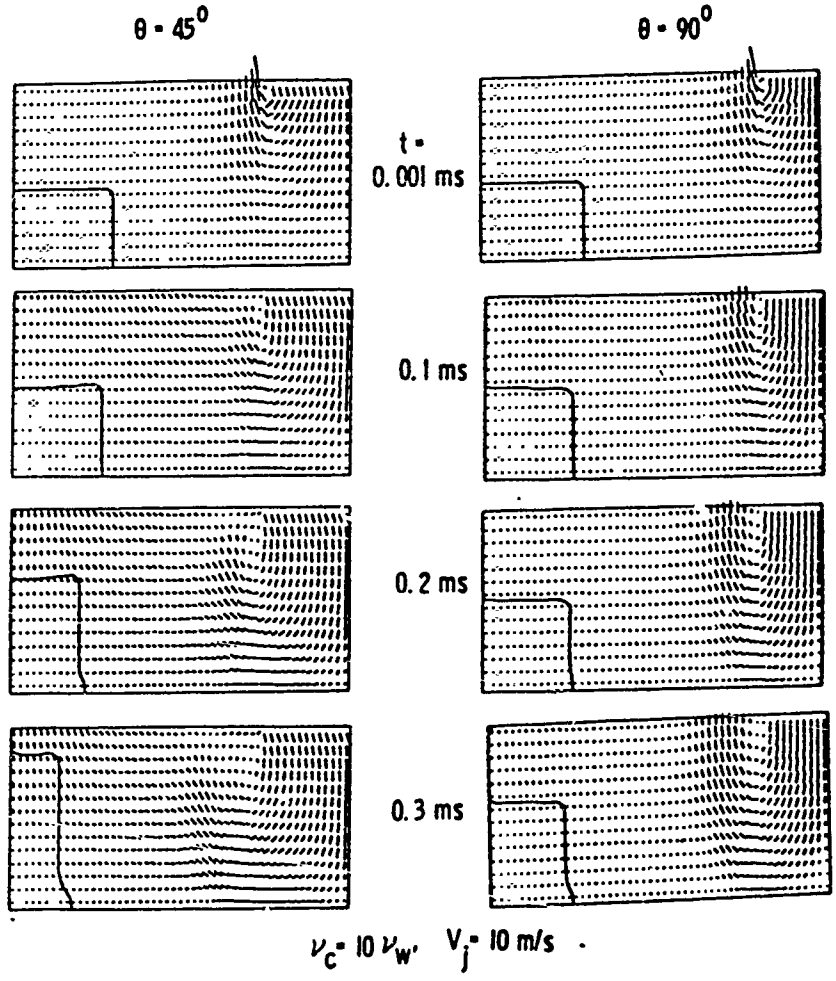

Fig. 8 Flow Development (corresponding to Fig. 2b)

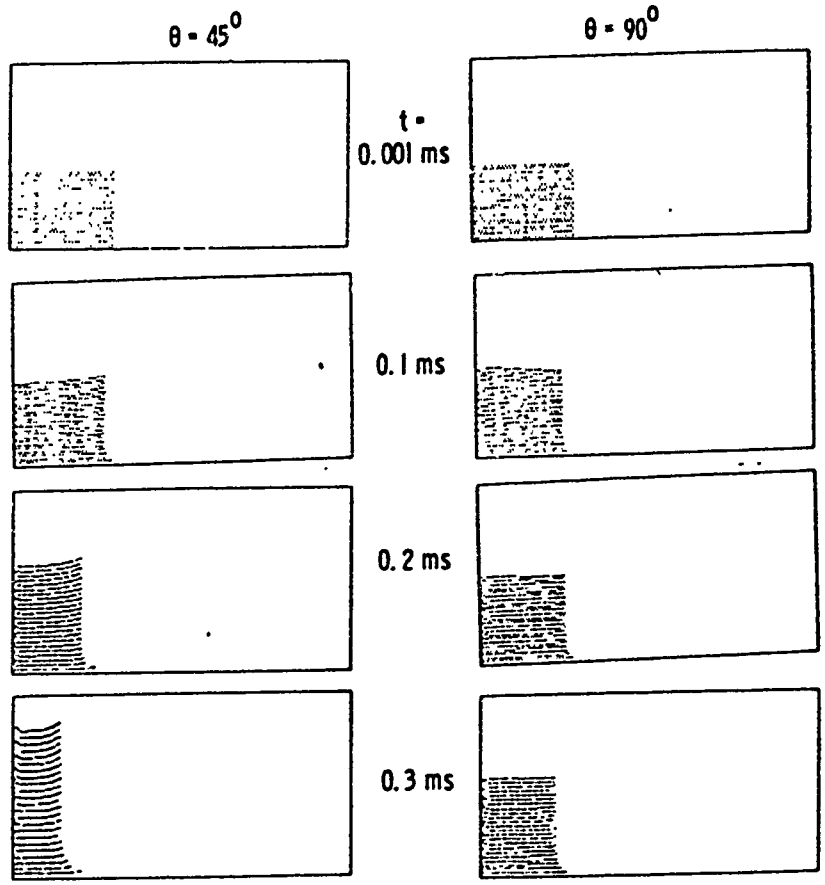

Fig. 9 Evolution of Drops (corresponding to Fig. 8)

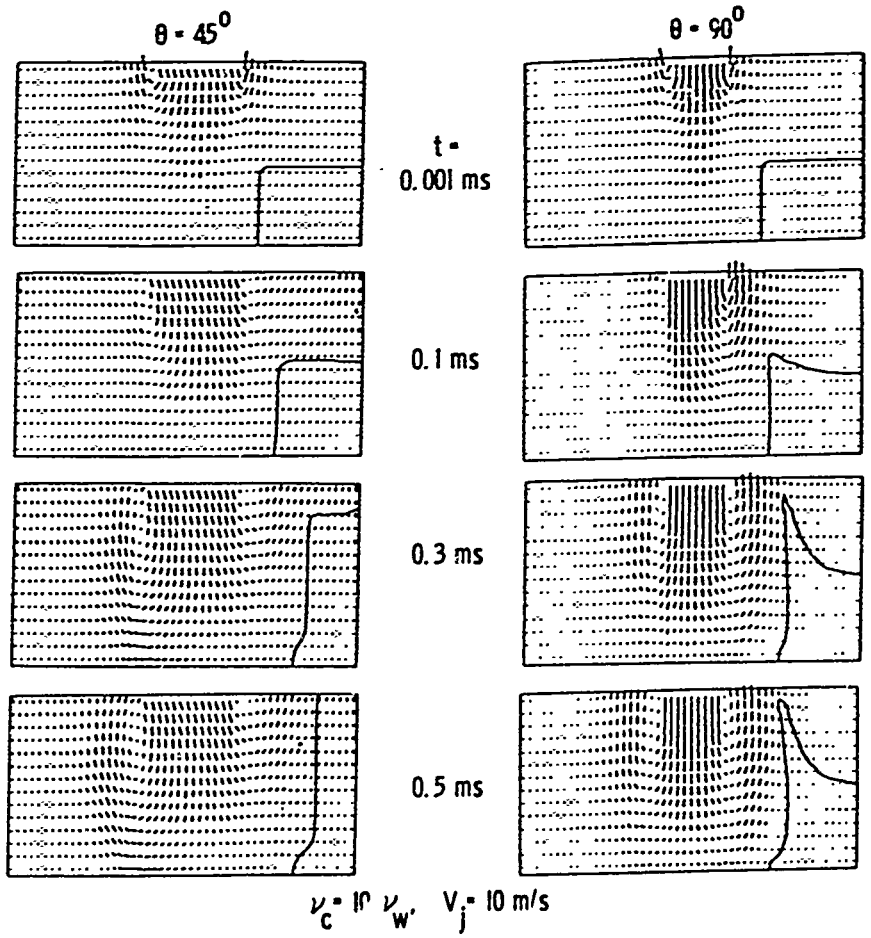

Fig. 10 Flow Development (corresponding to Fig. 2c)

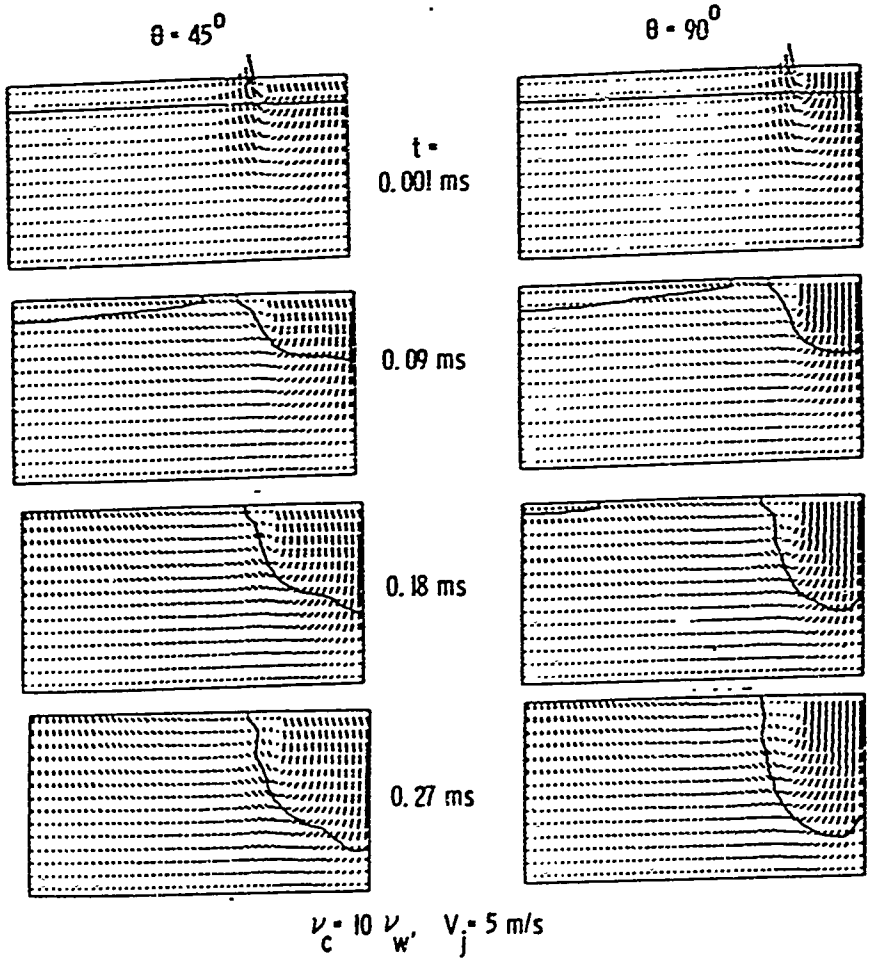

Fig. 11 Flow Development (corresponding to Fig. 2d)

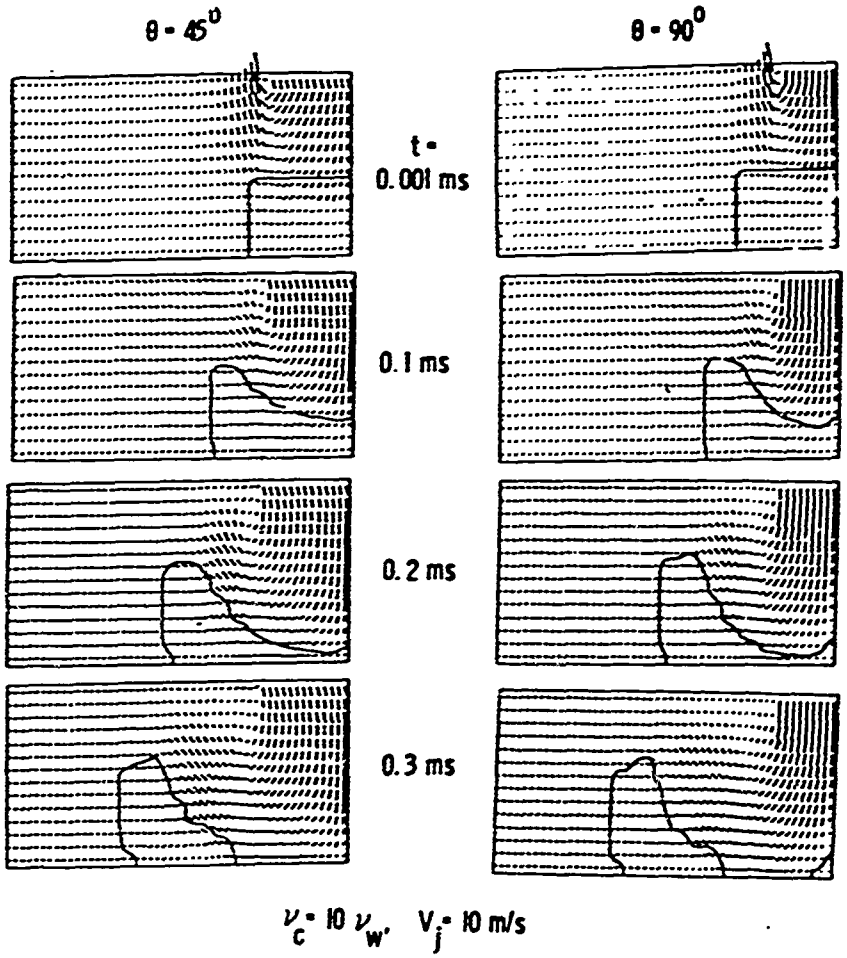

Fig. 12 Flow Development (corresponding to Fig. 3a)

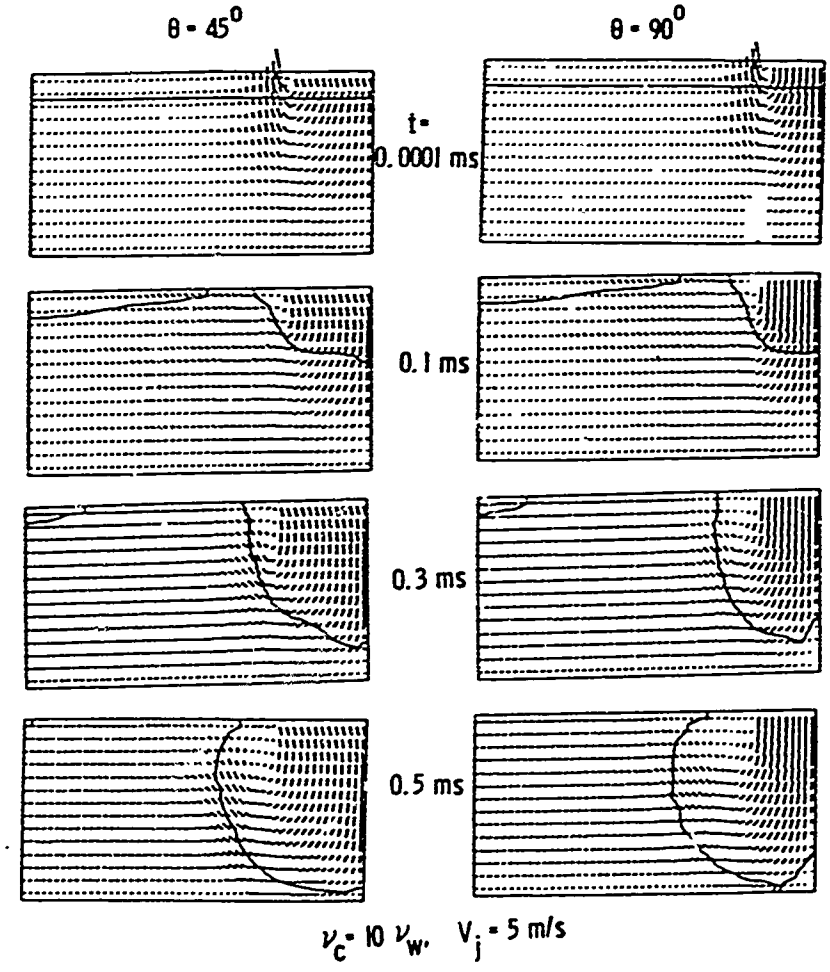

Fig. 13 Flow Development (corresponding to Fig. 3b)

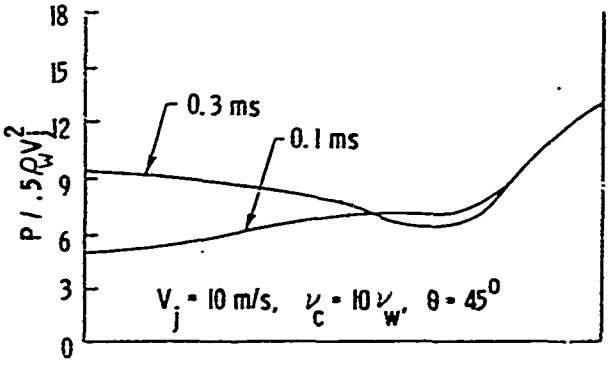

Fig. 14 Pressure Distribution on Bottom Wall Resulting from the Impingement of Fig. 2a

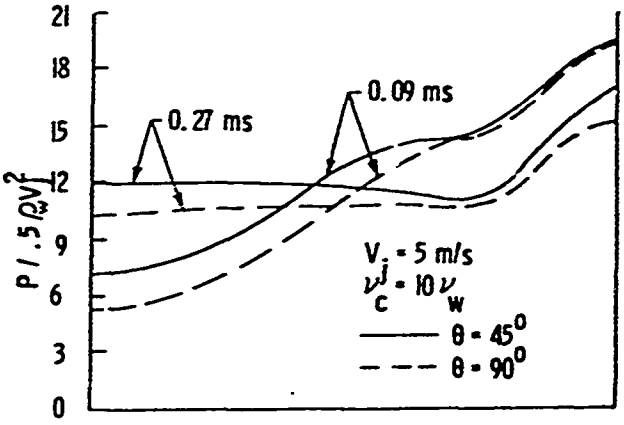

Fig. 15 Pressure Distribution on Bottom Wall Resulting from Impingement of Fig. 2d

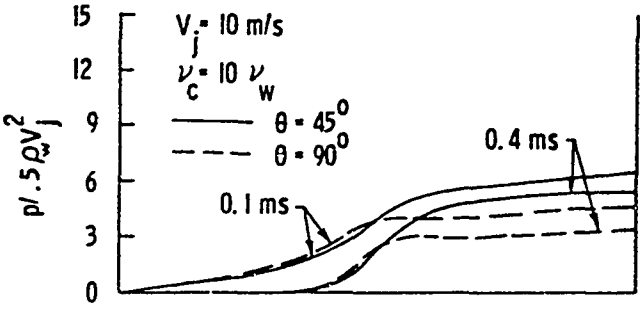

Fig. 16 Pressure Distribution on Bottom Wall Resulting from the Impingement of Fig. 3a

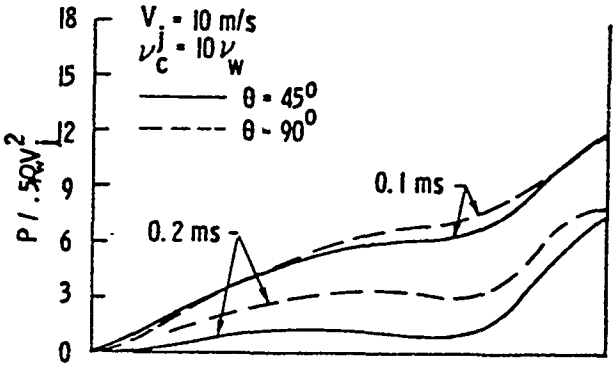

Fig. 17 Pressure Distribution on Bottom Wall Resulting from Impingement of Fig. 3b